# Quasi-two-dimensional superconductivity in $SnSe_2$ via organic ion intercalation

L. K. Ma,[1] M. Z. Shi,[1] B. L. Kang,[1] K. L. Peng,[1] F. B. Meng,[1] C. S. Zhu,[1] J. H. Cui,[1] Z. L. Sun,[1] D. H. Ma,[1] H. H. Wang,[1] B. Lei,[1,*] T. Wu,[1,2,3,4] and X. H. Chen[1,2,3,4,†]

[1]*Hefei National Laboratory for Physical Sciences at Microscale and Department of Physics, and CAS Key Laboratory of Strongly-coupled Quantum Matter Physics, University of Science and Technology of China, Hefei, Anhui 230026, China*

[2]*CAS Center for Excellence in Superconducting Electronics (CENSE), Shanghai 200050, China*

[3]*CAS Center for Excellence in Quantum Information and Quantum Physics, Hefei, Anhui 230026, China*

[4]*Collaborative Innovation Center of Advanced Microstructures, Nanjing University, Nanjing 210093, China*

(Received 4 June 2020; revised 10 August 2020; accepted 3 December 2020; published 17 December 2020)

In this work, two organic-ion-intercalated $SnSe_2$ superconductors, $(TBA)_xSnSe_2$ ($T_c \sim 6.4$ K) and $(CTA)_xSnSe_2$ ($T_c \sim 7.1$ K), are synthesized by an electrochemical intercalation method. Via the intercalation of organic ions, the interlayer distance is dramatically enlarged from 6.12 Å of pristine $SnSe_2$ to 18.62 and 14.74 Å for $(TBA)_xSnSe_2$ and $(CTA)_xSnSe_2$, respectively. Bulk magnetic susceptibility measurements suggest that both superconductors exhibit a strong anisotropic superconducting shielding effect below $T_c$. Further measurements of resistivity, *I-V* characteristic curves, and magnetoresistance reveal a quasi-two-dimensional (2D) superconductivity in $(CTA)_xSnSe_2$. The present work suggests that the organic-ion-intercalation method can induce quasi-2D superconductivity in $SnSe_2$ layers and provides a simple and practical strategy to explore 2D superconductivity as well as other 2D phenomena in layered materials.

DOI: 10.1103/PhysRevMaterials.4.124803

## I. INTRODUCTION

Exploring two-dimensional (2D) superconductivity in new layered materials has attracted significant research interest in condensed matter physics [1]. 2D superconductivity has been realized through various fabrication techniques, such as molecular beam epitaxy (MBE) [2,3], mechanical exfoliation [4,5], and the electric-double-layer transistor (EDLT) gating method [6,7]. Many emergent phenomena have been observed in these 2D superconducting systems, such as the quantum metallic state [8,9], quantum Griffiths singularity [10,11], and anomalously large upper critical field [12,13]. However, due to the complication of the fabrication techniques mentioned above, the fabrication of 2D systems from layered materials is still a challenge up to now. The electrochemical intercalation method can enlarge interlayer distance, which weakens the interlayer coupling and reduces the dimensionality of layered materials, providing an alternative way to manipulate electronic, magnetic, topological, and superconducting properties of van der Waals materials [14–17].

$SnSe_2$, crystallized in the $CdI_2$-type 1T structure, is an intrinsic semiconductor with a band gap of 1.0 eV at room temperature [18]. Superconductivity can be induced through various methods in this layered material [19–27], and interplay between superconductivity and charge density wave (CDW) or ferromagnetism has also been reported in this system [19–21]. Besides, 2D superconductivity has been demonstrated in $SnSe_2$/ionic liquid interface and $SnSe_2$/graphene heterostructure [24,25]. Recently, by co-intercalation of organic molecules and lithium ions into $SnSe_2$, various superconducting materials with dramatically enlarged interlayer distance have been reported [27]. Up to now, whether 2D superconductivity induced by dimensional crossover from three dimensions to two dimensions owing to intercalation exists or not is still elusive.

Here, we report quasi-2D superconductivity in organic-ion-intercalated $SnSe_2$ superconductors. Via the electrochemical intercalation method, two $SnSe_2$-based superconductors with dramatically enlarged interlayer distance, namely $(TBA)_xSnSe_2$ and $(CTA)_xSnSe_2$, are archived. Measurements of magnetic susceptibility indicate that both materials display strong anisotropic superconducting shielding effect below $T_c$. Anisotropic resistivity, *I-V* characteristic curves, and magnetoresistance measurements further support quasi-2D superconductivity in $(CTA)_xSnSe_2$. All experimental results indicate that organic-ion-intercalated $SnSe_2$ materials exhibit quasi-2D superconductivity and suggest that the organic-ion-intercalation method can be exploited to investigate emergent 2D proprieties in layered materials.

## II. EXPERIMENTAL METHODS

To synthesize pristine $SnSe_2$ single crystal, Sn powder (grain size: 1–6 $\mu$m, 99.999%) and Se powder (grain size: 1–6 $\mu$m, 99.999%) were weighed according to the stoichiometry of $SnSe_2$ and loaded into a cone-shaped silica tube and flame-sealed at a pressure of $\sim 10^{-3}$ Pa. The silica tube was placed in a modified Bridgeman furnace, slowly heated up to 1100 K over 8 h, and then slowly cooled to 1000 K with 3 h and soaked at this temperature for 4 days with the sample moving at a rate of 1.5 mmh$^{-1}$. $SnSe_2$ single crystals with typical size of 13 mm (diameter) × 40 mm (length) were readily obtained.

*Corresponding author: leibin@ustc.edu.cn
†Corresponding author: chenxh@ustc.edu.cn

 

Each piece of $SnSe_2$ single crystal was accurately weighted with a high-accuracy balance (Mettler Toledo AX26), and then fixed onto an indium plate as the positive electrode. The negative electrode is composed of a silver piece. The electrolyte was obtained by dissolving 6-g TBAB (tetrabutyl ammonium bromide, Aladdin, 99.0%) or 300-mg CTAB (hexadecyl trimethyl ammonium bromide, Innochem, 99%) powder in 20-mL DMF (dimethylformamide, Innochem, 99.9%, extra dry with molecular sieves, water less than 50 ppm) and the intercalation process was conducted in this liquid solution. The electrolytic cell was placed into an argon-filled glovebox with the $O_2$ and $H_2O$ levels below 1 ppm and the intercalation process was controlled by a Lanhe testing system with a current of 10–20 $\mu$A during a calculated time $t$. When the current passes through the electrolytic cell, the negative electrode loses electrons, and the positive electrode obtains electrons. The electrochemical reaction can be described as the following equations:

$$\mathrm{Br}^- + \mathrm{Ag} \rightarrow \mathrm{AgBr} + e^-,$$

$$\mathrm{SnSe_2} + xe^- + x\mathrm{TBA}^+ \rightarrow (\mathrm{TBA})_x\mathrm{SnSe_2}[\text{or } \mathrm{SnSe_2} + xe^- + x\mathrm{CTA}^+ \rightarrow (\mathrm{CTA})_x\mathrm{SnSe_2}].$$

The amount of intercalated $TBA^+$ (or $CTA^+$), namely $x$ in $(TBA)_xSnSe_2$ (or $(CTA)_xSnSe_2$), was calculated according to the following formula:

$$t = Fmx/MI,$$

where $t$ is the time (s), $F$ is the Farady constant (96 485.31 C $mol^{-1}$), $m$ is the mass (g) of pristine $SnSe_2$ single crystal, $x$ is the amount of intercalated $TBA^+$ (or $CTA^+$), $M$ is the molar mass (g $mol^{-1}$) of $SnSe_2$, and $I$ is the electric current (A) passing through the cell.

The crystal structure was characterized by an x-ray diffractometer (Rigaku SmartLab 9 KW) equipped with Cu $K\alpha$ radiation and a fixed graphite monochromator. The magnetic susceptibility measurement was carried out with a superconducting quantum interference device magnetometer (Quantum Design MPMS-5). The resistivity measurement was conducted on a physical property measurement system (Quantum Design PPMS-9T) with the standard four-terminal method. To prevent damage from oxygen and moisture, the preparation for measurements was conducted in an argon-filled glovebox and the crystal was measured as soon as the preparation was completed.

## III. RESULTS AND DISCUSSION

High quality $SnSe_2$ single crystal was selected as the host material to conduct the electrochemical intercalation. The top and side views of $SnSe_2$ crystal structure are shown on the left side of Fig. 1(b). The Sn layer is sandwiched be-

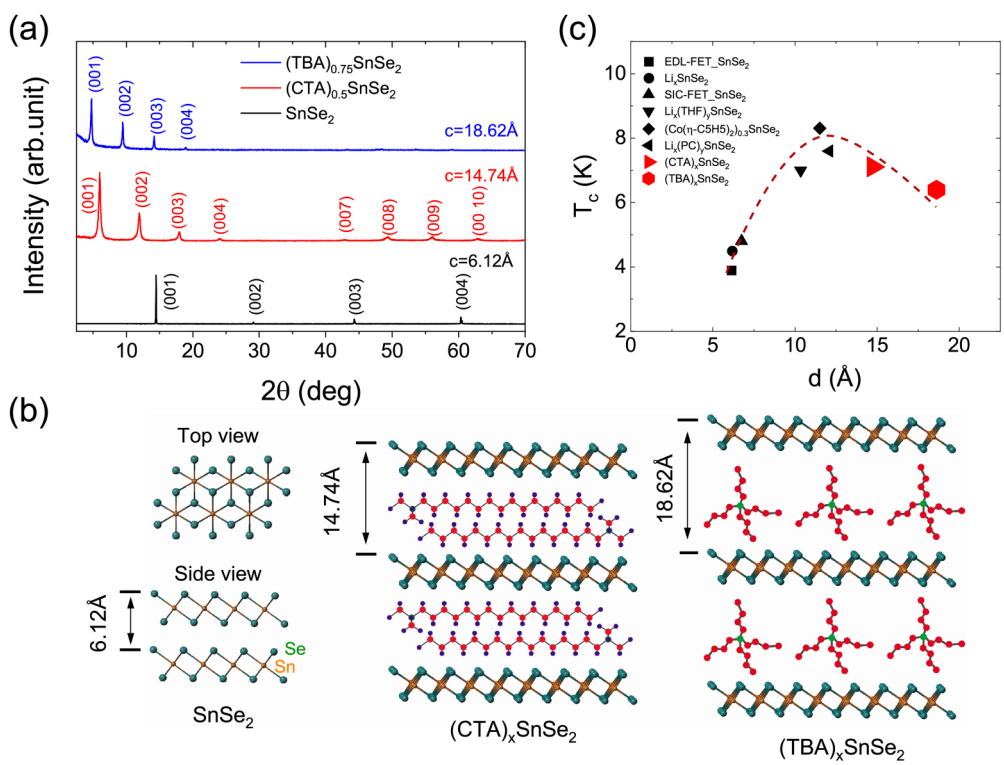


FIG. 1. (a) X-ray diffraction patterns of $(TBA)_{0.75}SnSe_2$, $(CTA)_{0.5}SnSe_2$, and $SnSe_2$. All the samples show a series of (00 $l$) diffraction peaks and the diffraction peak positions do not move with changing $x$ for intercalated samples [see Figs. S2(a) and S2(b) in Supplemental Material [28]]. So, only XRD patterns of $(TBA)_{0.75}SnSe_2$ and $(CTA)_{0.5}SnSe_2$ are chosen to present in (a). The interlayer distance of resulting organic-ion-intercalated samples are enlarged from 6.12 to 18.62 and 14.74 Å for $(TBA)_xSnSe_2$ and $(CTA)_xSnSe_2$, respectively. (b) The schematic crystal structure of pristine $SnSe_2$, $(CTA)_xSnSe_2$ and $(TBA)_xSnSe_2$. (c) Superconducting transition temperature $T_c$ vs interlayer distance $c$ in various $SnSe_2$ superconductors [20,24,26,27]. Black symbols: earlier data. Red symbols: this work. The red dash line is a guide for the domelike behavior of $T_c$ vs $d$.

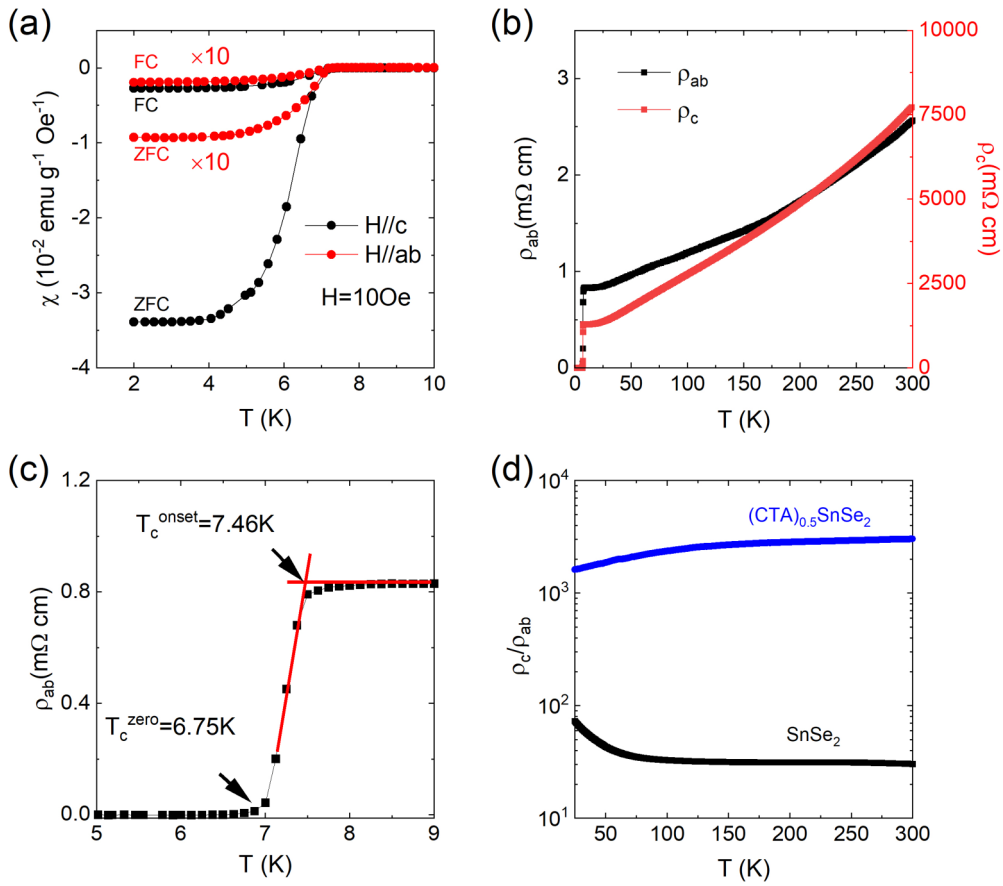


FIG. 2. (a) Temperature-dependent magnetic susceptibility of $(CTA)_{0.5}SnSe_2$. The curves are measured in both zero-field cooled (ZFC) and field cooled (FC) modes with magnetic field of 10 Oe applied along in-plane (red) and out-of-plane (black) directions. For clarity, the red curves are enlarged by ten times. (b) Temperature-dependent in-plane (black) and out-of-plane (red) resistivity of $(CTA)_{0.5}SnSe_2$. (c) Enlarged views of $\rho_{ab}(T)$ around superconducting region. $T_c^{\text{onset}}$, onset critical temperature, defined as the intersection between the linear extrapolation of the normal state and the superconducting transition. $T_c^{\text{zero}}$, zero resistance temperature. (d) Temperature-dependent anisotropy of resistivity $(\rho_c/\rho_{ab})$ for $(CTA)_{0.5}SnSe_2$ (blue) and $SnSe_2$ (black).

tween two Se layers with Sn-Se-Sn atomic stacking. A Sn atom is surrounded by six Se atoms, forming an octahedral coordination. The distance between two adjacent $SnSe_2$ layers is 6.12 Å. Figure 1(a) shows the x-ray diffraction (XRD) patterns for pristine and electrochemical intercalated $SnSe_2$ crystals. From the galvanostatic discharge curves of $(TBA)_xSnSe_2$ [$(CTA)_xSnSe_2$] [see Fig. S1 in the Supplemental Material [28]], the maximum $x$ for $(TBA)_xSnSe_2$ [$(CTA)_xSnSe_2$] is estimated to be 1.28 (1.12). Although the amounts of intercalated organic ions are different, the diffraction peak positions show no obvious difference for each kind of organic-ion-intercalated samples [see Figs. S2(a) and S2(b) in the Supplemental Material [28]]. As shown in Fig. 1(a), all the samples show clear (00 $l$) diffraction peaks and the interlayer distance is enlarged from 6.12 Å of pristine crystal to 18.62 Å for $(TBA)_xSnSe_2$ and 14.74 Å for $(CTA)_xSnSe_2$, respectively. Considering the size of $TBA^+$ (8.4–11.9 Å) and $CTA^+$ (4.1–4.6 Å) [see Fig. S3 in the Supplemental Material [28]], the proposed structure models for intercalated products are illustrated in Fig. 1(b). For $(TBA)_xSnSe_2$, the interlayer distance of 18.62 Å is the sum of single layer $SnSe_2$ and one layer of $TBA^+$ cations. As for $(CTA)_xSnSe_2$, two layers of $CTA^+$ cations can be intercalated into $SnSe_2$ to enlarge the interlayer distance from 6.12 to 14.74 Å. Temperature-dependent magnetic susceptibility measurements on both materials show obvious diamagnetism below 6.4 and 7.1 K for $(TBA)_xSnSe_2$ and $(CTA)_xSnSe_2$ [see Figs. S4(a) and S4(b) in the Supplemental Material [28]], indicating the appearance of superconductivity. It is interesting that the amount of intercalated organic ions has little influence on $T_c$, but can affect the superconducting shielding fraction. Similar results have been observed in previous intercalated $SnSe_2$ materials, probably suggesting doping independent $N(0)$ characteristics of a nearly free electron 2D system [27]. Through the organic-ion-intercalation method, two $SnSe_2$-based superconductors, $(TBA)_xSnSe_2$ and $(CTA)_xSnSe_2$, are synthesized. By adding these two new members into $SnSe_2$-based superconductors, an interesting $T_c$ vs interlayer spacing $d$ phase diagram of the $SnSe_2$ family is established in Fig. 1(c), where the $T_c$ shows a domelike behavior with increasing $d$ in this system. Similar $T_c$ vs $d$ behavior has also been observed in intercalated HfNCl superconductors [29]. The domelike behavior observed here suggests that some similar mechanism may play an important role behind them, irrespective of the electronic states in the parent materials. It is noteworthy that our organic-ion-intercalated materials have the largest interlayer distance

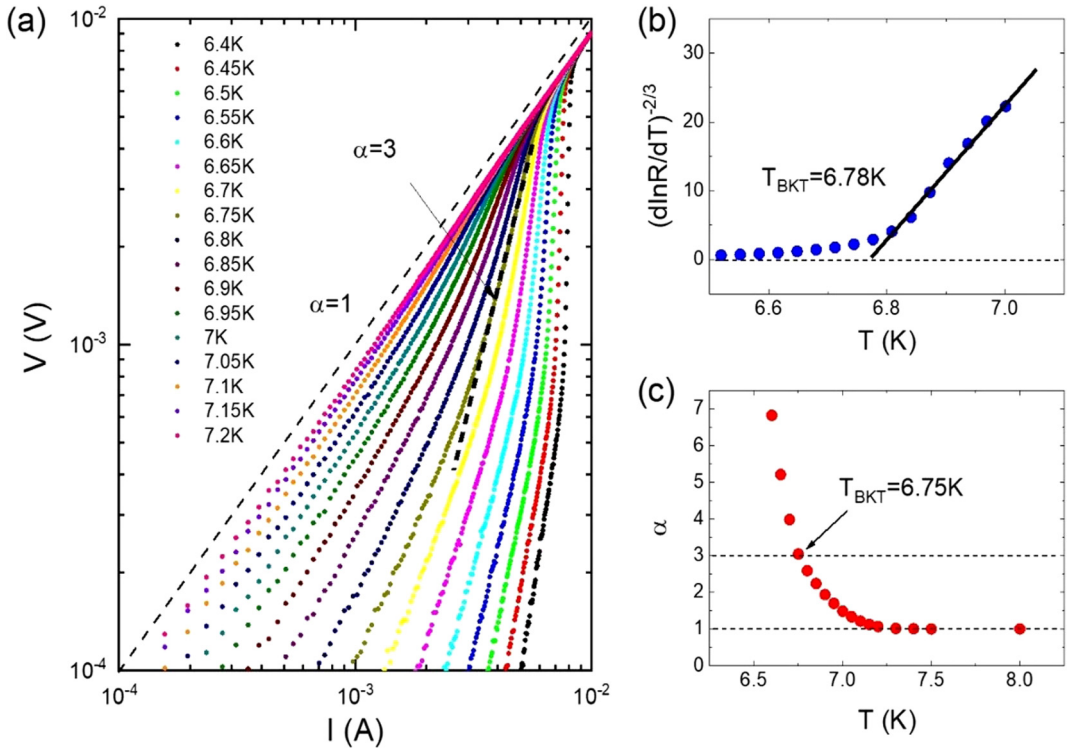


FIG. 3. (a) The *V-I* relationship at different temperatures in superconducting regime for $(CTA)_{0.5}SnSe_2$. The curves are plotted on a logarithmic scale. The two black dot lines denote to $V \sim I$ and $V \sim I^3$, respectively. (b) $R(T)$ dependent $(CTA)_{0.5}SnSe_2$ sample, plotted on a $[d\ln R/dT]^{-2/3}$ scale. The solid black line is the behavior expected for a BKT transition with $T_{BKT} = 6.78$ K. (c) Temperature-dependent $\alpha$ from fitting the power law dependent $V \sim I^{\alpha}$ from (a). $T_{BKT} = 6.75$ K is obtained for $\alpha = 3$.

among all the $SnSe_2$-based superconductors. As a result of the dramatically increased interlayer distance, dimensional crossover from 3D to 2D could be expected in these two intercalated materials.

For 2D superconductors, the diamagnetic signals with magnetic field parallel to superconducting layers should be much smaller than that with magnetic field perpendicular to superconducting layers. Figure 2(a) shows the temperature-dependent magnetic susceptibility of $(CTA)_{0.5}SnSe_2$ with magnetic field applied along the in-plane and out-of-plane directions, respectively. Indeed, a significant change of the superconducting shielding fraction with magnetic field applied from the in-plane to the out-of-plane direction is observed, indicating the 2D-like nature of superconductivity in $(CTA)_{0.5}SnSe_2$. Magnetic susceptibility measurements on $(TBA)_{0.75}SnSe_2$ suggest that $TBA^+$ intercalated $SnSe_2$ products also exhibit strong anisotropic superconducting shielding effect below $T_c$ [see Fig. S4(c) in the Supplemental Material [28]]. With weakened interlayer coupling, organic-ion-intercalated $SnSe_2$ products should exhibit a 2D-like characteristic in electric transport properties. The $TBA^+$ intercalated $SnSe_2$ samples cannot maintain original morphology after intercalation, and are difficult to conduct electric transport measurements. Therefore, $(CTA)_xSnSe_2$ is chosen to conduct further measurements to investigate the electric transport proprieties. Temperature-dependent in-plane and out-of-plane resistivity of $(CTA)_{0.5}SnSe_2$ are shown in Fig. 2(b). With cooling down, the resistivity of $(CTA)_{0.5}SnSe_2$ decreases monotonously, in contrast to the pristine semiconducting $SnSe_2$ [see Fig. S5 in the Supplemental Material [28]]. With further decreasing temperature, the resistivity drops sharply at 7.46 K (onset critical temperature, $T_c^{\text{onset}}$), and approaches to zero at 6.75 K (zero resistance temperature, $T_c^{\text{zero}}$) [see Fig. 2(c)]. The temperature-dependent anisotropic resistivity $\rho_c/\rho_{ab}$ for $(CTA)_{0.5}SnSe_2$ and $SnSe_2$ is plotted in Fig. 2(d). Compared to pristine $SnSe_2$, the value of $\rho_c/\rho_{ab}$ is enlarged by two orders of magnitude owing to the weak interlayer coupling due to the intercalation of organic ions, which supports a 2D-like electronic structure of $(CTA)_{0.5}SnSe_2$.

To further verify the 2D-like superconductivity in $(CTA)_{0.5}SnSe_2$, we measured the temperature-dependent *I-V* curves around $T_c^{\text{zero}}$. In 2D superconductors, the transition into the superconducting state would be a Berezinskii-Kosterlitz-Thouless (BKT) transition, characterized by a transition temperature $T_{BKT}$ at which vortex-antivortex pairs unbind [30]. At the BKT transition, the current-induced Lorentz force causes vortex-antivortex pairs unbinding, resulting in a $V \sim I^{\alpha}$ behavior with $\alpha(T_{BKT}) = 3$ [31]. As shown in Fig. 3(a), our sample shows the power law dependent behavior with $V \sim I^{\alpha}$, which is a distinct signature of the BKT transition. The temperature-dependent power law exponent $\alpha$, deduced from the linear fitting of the *V-I* curves, is shown in Fig. 3(c). With decreasing temperature, $\alpha$ gradually increases. At the BKT transition temperature, $T_{BKT} = 6.75$ K, $\alpha$ equals 3. Moreover, the temperature-dependent resistance $R(T)$ follows a typical BKT-like behavior with $R(T) = R_0\exp[-b/(T - T_{BKT})^{1/2}]$ in the temperature range close to $T_{BKT}$, where $R_0$ and $b$ are material dependent param-

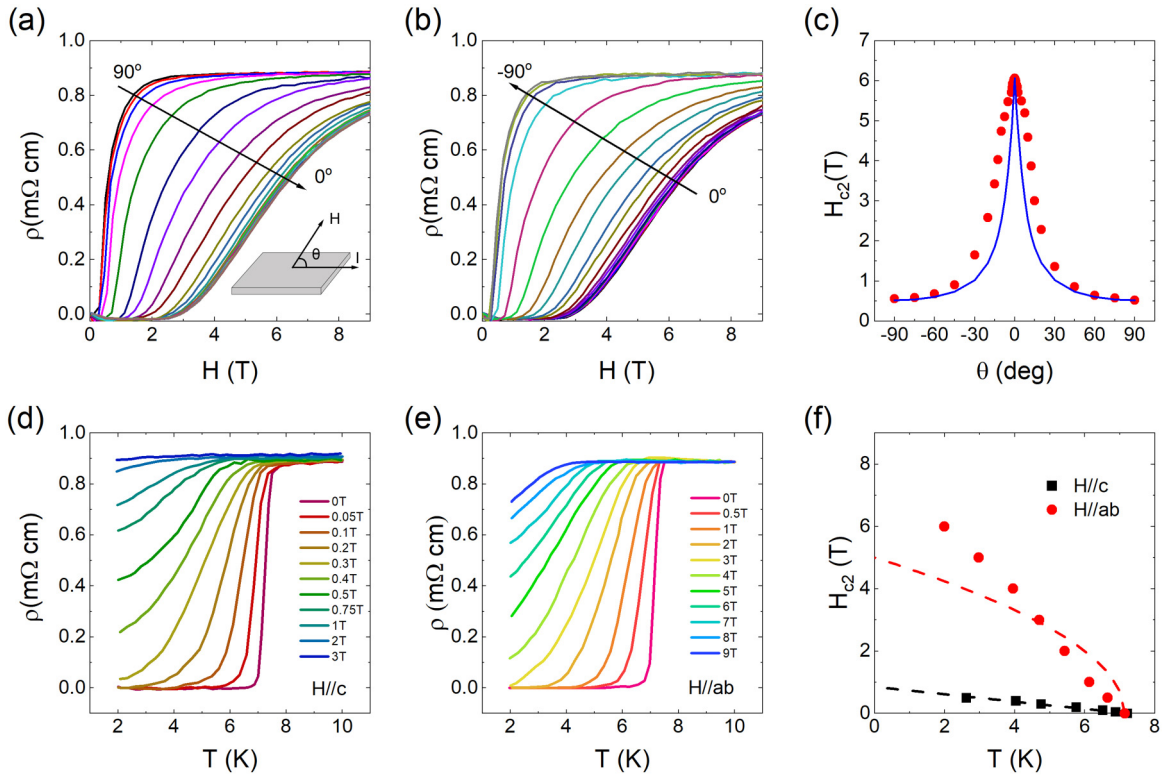


FIG. 4. (a), (b) Angular-dependent $\rho(T)$ at 2 K for $(CTA)_{0.5}SnSe_2$. In the inset, $\theta$ is the angle between the magnetic field and the sample surface. (c) Angular-dependent upper critical field ($H_{c2}$, defined as the magnetic field where the resistivity equals half value of the normal state) with $\theta$ from 90° to −90°. The blue solid line is fit to the 2D Tinkham formula, $(\frac{H_{c2}(\theta)\cos(\theta)}{H_{c2}^{ab}})^2 + |\frac{H_{c2}(\theta)\sin(\theta)}{H_{c2}^{c}}| = 1$, where $H_{c2}^{ab}$ and $H_{c2}^{c}$ are the upper critical fields at $\theta = 0°$ and 90°. (d), (e) Temperature-dependent resistivity under a constant out-of-plane and in-plane magnetic field. (f) Temperature-dependent $H_{c2}$ with magnetic field applied along out-of-plane (black) and in-plane (red) directions. The black and red dash line are fits to 2D Ginzburg-Landau model, $H_{c2}^{c}(T) = \frac{\Phi_0}{2\pi\xi_{GL}(0)^2}(1 - \frac{T}{T_c})$, $H_{c2}^{ab}(T) = \frac{\Phi_0\sqrt{12}}{2\pi\xi_{GL}(0)d_{sc}}(1 - \frac{T}{T_c})^{1/2}$, where $\Phi_0$ is the magnetic flux quantum, $\xi_{GL}(0)$ is the in-plane 2D GL coherence length at 0 K, and $d_{sc}$ is the thickness of the superconductor.

eters [32]. As shown in Fig. 3(b), the extracted value of $T_{BKT}$ from the measured $R(T)$ curve is about 6.78 K, in agreement with the analysis on $V \sim I^{\alpha}$. All the experimental results here support a 2D-like superconductivity in $(CTA)_{0.5}SnSe_2$.

Considering the 2D-like superconductivity in $(CTA)_{0.5}SnSe_2$, the superconducting state should be much more robust against the in-plane magnetic field than the out-of-plane magnetic field. Figures 4(a) and 4(b) show magnetoresistance at various $\theta$ [defined as the angle between the magnetic field and sample surface, as illustrated in the inset of Fig. 4(a)] at 2 K for $(CTA)_{0.5}SnSe_2$. The magnetoresistance is highly $\theta$ dependent. The magnetoresistance at $\theta = 90°$ approaches saturation within 2 T, whereas even up to 9 T, the magnetoresistance at $\theta = 0°$ does not show any signatures of saturation. The upper critical magnetic field $H_{c2}$ (defined as the magnetic field where the resistivity equals the half value of the normal state) at various $\theta$, extracted from Figs. 4(a) and 4(b), is plotted in Fig. 4(c). With the magnetic field rotating from the out-of-plane direction to the in-plane direction, $H_{c2}$ increases from 0.5 to 6 T. Although above strong anisotropy of $H_{c2}$ is expected for 2D superconductivity, the angular-dependent $H_{c2}$ can't be fitted by standard 2D Tinkham formula [33]. Compared to the gating-induced interface superconductivity in $SnSe_2$ [24], our data show a much more rounded feature around $\theta = 0°$. This behavior probably results from the degradation of unruffled layers in our materials, which can also be found in other organic-ion-intercalated materials [14–16] and is further supported by the broadening of full width at half maximum in the rocking curve of the (001) reflection after $CTA^+$ intercalation [see Fig. S6 in the Supplemental Material [28]]. Figures 4(d) and 4(e) display the temperature-dependent resistivity under different out-of-plane and in-plane magnetic fields. When the magnetic field is applied along the out-of-plane direction, superconductivity is completely suppressed down to 2 K under 3 T, while superconductivity can survive even up to 9 T with the magnetic field applied along the in-plane direction. Compared to 2D superconductivity in the $SnSe_2$ EDLT device [24], the superconducting transition of $(CTA)_{0.5}SnSe_2$ broadens with increasing magnetic field, indicating a much more active dynamics of vortices in our intercalated material. The temperature-dependent $H_{c2}$, also defined as the magnetic field where the resistivity equals the half value of the normal state, and the corresponding fitting curves using 2D Ginzburg-Landau theory are plotted in Fig. 4(f). Instead of $H_{c2}^{ab}(T) \propto (1 - \frac{T}{T_c})^{1/2}$, $H_{c2}^{ab}$ displays linearlike behavior with temperature cooling down. Notably, neither $\theta$-dependent nor $T$-dependent $H_{c2}$ can be well described by the 2D standard model, indicating that perfect 2D superconducting behavior

is not truly observed in our samples, which is probably due to either the degradation of unruffled $SnSe_2$ layers or the weak coupling between adjacent $SnSe_2$ layers in our intercalated products. The true 2D superconductivity could be expected in samples with larger organic ion intercalation as well as smoother $SnSe_2$ layers. Anyway, our experimental results suggest that quasi-2D superconductivity can be achieved in organic-ion-intercalated $SnSe_2$.

## IV. CONCLUSION

In conclusion, we synthesize two organic-ion-intercalated $SnSe_2$ superconductors, namely $(TBA)_xSnSe_2$ and $(CTA)_xSnSe_2$, by an organic-ion-intercalation method. With dramatically enlarged interlayer distance, both materials show strong anisotropic superconducting shielding effect below $T_c$. Further electric transport measurements on $(CTA)_xSnSe_2$, such as anisotropic resistivity, *I-V* characteristic curves, and magnetoresistance measurements, demonstrate quasi-2D superconductivity in $(CTA)_xSnSe_2$. Our work indicates that organic-ion-intercalated $SnSe_2$ superconductors display quasi-2D superconductivity and suggests that the organic-ion-intercalation method can be exploited as an alternative method to explore 2D novel phenomena in van der Waals materials.

## ACKNOWLEDGMENTS

This work was supported by the National Key Research and Development Program of the Ministry of Science and Technology of China (Grants No. 2017YFA0303001, No. 2016YFA0300201 and No. 2019YFA0704901), the Strategic Priority Research Program of Chinese Academy of Sciences (Grant No. XDB25000000), the National Natural Science Foundation of China (Grants No. 11888101 and No. 11534010), Anhui Initiative in Quantum Information Technologies (Grant No. AHY160000), the Science Challenge Project of China (Grant No. TZ2016004), and the Key Research Program of Frontier Sciences, CAS, China (Grant No. QYZDYSSW-SLH021).

[1] Y. Saito, T. Nojima, and Y. Iwasa, Nat. Rev. Mater. **2**, 16094 (2016).
[2] Q. Y. Wang, Z. Li, W. H. Zhang, Z. C. Zhang, J. S. Zhang, W. Li, H. Ding, Y. B. Ou, P. Deng, K. Chang, J. Wen, C. L. Song, K. He, J. F. Jia, S. H. Ji, Y. Y. Wang, L. L. Wang, X. Chen, X. C. Ma, and Q. K. Xue, Chin. Phys. Lett. **29**, 37402 (2012).
[3] S. Y. Qin, J. Kim, Q. Niu, and C.-K. Shih, Science **324**, 1314 (2009).
[4] D. Jiang, T. Hu, L. X. You, Q. Li, A. Li, H. M. Wang, G. Mu, Z. Y. Chen, H. R. Zhang, G. H. Yu, J. Zhu, Q. J. Sun, C. T. Lin, H. Xiao, X. M. Xie, and M. H. Jiang, Nat. Commun. **5**, 5708 (2014).
[5] X. X. Xi, L. Zhao, Z. F. Wang, H. Berger, L. Forró, J. Shan, and K. F. Mak, Nat. Nanotechnol. **10**, 765 (2015).
[6] K. Ueno, S. Nakamura, H. Shimotani, A. Ohtomo, N. Kimura, T. Nojima, H. Aoki, Y. Iwasa, and M. Kawasaki, Nat. Mater. **7**, 855 (2008).
[7] J. T. Ye, Y. J. Zhang, R. Akashi, M. S. Bahramy, R. Arita, and Y. Iwasa, Science **338**, 1193 (2012).
[8] Y. Saito, Y. Kasahara, J. T. Ye, Y. Iwasa, and T. Nojima, Science **350**, 409 (2015).
[9] A. W. Tsen, B. Hunt, Y. D. Kim, Z. J. Yuan, S. Jia, R. J. Cava, J. Hone, P. Kim, C. R. Dean, and A. N. Pasupathy, Nat. Phys. **12**, 208 (2016).
[10] Y. Xing, H. M. Zhang, H. L. Fu, H. W. Liu, Y. Sun, J. P. Peng, F. Wang, X. Lin, X. C. Ma, Q. K. Xue, J. Wang, and X. C. Xie, Science **350**, 542 (2015).
[11] S. Sachdev, P. Werner, and M. Troyer, Phys. Rev. Lett. **92**, 237003 (2004).
[12] X. X. Xi, Z. F. Wang, W. W. Zhao, J. H. Park, K. T. Law, H. Berger, L. Forró, J. Shan, and K. F. Mak, Nat. Phys. **12**, 139 (2016).
[13] J. M. Lu, O. Zheliuk, I. Leermakers, N. F. Q. Yuan, U. Zeitler, K. T. Law, and J. T. Ye, Science **350**, 1353 (2015).
[14] M. Z. Shi, N. Z. Wang, B. Lei, C. Shang, F. B. Meng, L. K. Ma, F. X. Zhang, D. Z. Kuang, and X. H. Chen, Phys. Rev. Mater. **2**, 074801 (2018).
[15] M. Z. Shi, N. Z. Wang, B. Lei, J. J. Ying, C. S. Zhu, Z. L. Sun, J. H. Cui, F. B. Meng, C. Shang, L. K. Ma, and X. H. Chen, New J. Phys. **20**, 123007 (2018).
[16] N. Z. Wang, H. B. Tang, M. Z. Shi, H. Zhang, W. Z. Zhuo, D. Y. Liu, F. B. Meng, L. K. Ma, J. J. Ying, L. J. Zou, Z. Sun, and X. H. Chen, J. Am. Chem. Soc. **141**, 17166 (2019).
[17] H. X. Zhang, A. Rousuli, S. C. Shen, K. Zhang, C. Wang, L. P. Luo, J. Z. Wang, Y. Wu, Y. Xu, W. H. Duan, H. Yao, P. Yu, and S. Y. Zhou, Sci. Bull. **65**, 188 (2019).
[18] V. Bhatt, K. Gireesan, and G. Pandya, J. Cryst. Growth **96**, 649 (1989).
[19] C. A. Formstone, E. T. FitzGerald, D. O'Hare, P. A. Cox, M. Kurmoo, J. W. Hodby, D. Lillicrap, and M. Goss-Custard, J. Chem. Soc., Chem. Commun. 501 (1990).
[20] D. O'Hare, H. V. Wong, S. Hazell, and J. W. Hodby, Adv. Mater. **4**, 658 (1992).
[21] Z. J. Li, Y. C. Zhao, K. J. Mu, H. Shan, Y. Q. Guo, J. J. Wu, Y. Q. Su, Q. R. Wu, Z. Sun, A. D. Zhao, X. F. Cui, C. Z. Wu, and Y. Xie, J. Am. Chem. Soc. **139**, 16398 (2017).
[22] Y. H. Zhou, B. W. Zhang, X. L. Chen, C. C. Gu, C. An, Y. Zhou, K. M. Cai, Y. F. Yuan, C. H. Chen, H. Wu, R. R. Zhang, C. Y. Park, Y. M. Xiong, X. W. Zhang, K. Y. Wang, and Z. R. Yang, Adv. Electron. Mater. **4**, 1800155 (2018).
[23] Z. B. Shao, Z. G. Fu, S. J. Li, Y. Cao, Q. Bian, H. G. Sun, Z. Y. Zhang, H. Gedeon, X. Zhang, L. J. Liu, Z. W. Cheng, F. W. Zheng, P. Zhang, and M. H. Pan, Nano Lett. **19**, 5304 (2019).
[24] J. W. Zeng, E. F. Liu, Y. J. Fu, Z. Y. Chen, C. Pan, C. Y. Wang, M. Wang, Y. J. Wang, K. Xu, S. H. Cai, X. X. Yan, Y. Wang, X. W. Liu, P. Wang, S. J. Liang, Y. Cui, H. Y. Hwang, H. T. Yuan, and F. Miao, Nano Lett. **18**, 1410 (2018).

[25] Y. M. Zhang, J. Q. Fan, W. L. Wang, D. Zhang, L. L. Wang, W. Li, K. He, C. L. Song, X. C. Ma, and Q. K. Xue, Phys. Rev. B **98**, 220508(R) (2018).

[26] Y. P. Song, X. W. Liang, J. G. Guo, J. Deng, G. Y. Gao, and X. L. Chen, Phys. Rev. Mater. **3**, 054804 (2019).

[27] H. L. Wu, S. Li, M. Susner, S. Kwon, M. Kim, T. Haugan, and B. Lv, 2D Mater. **6**, 045048 (2019).

[28] See Supplemental Material at http://link.aps.org/supplemental/10.1103/PhysRevMaterials.4.124803 for more details about the preparation and characterization of $(CTA)_xSnSe_2$ and $(TBA)_xSnSe_2$ samples.

[29] K. Hotehama, T. Koiwasaki, K. Umemoto, S. Yamanaka, and H. Tou, J. Phys. Soc. Jpn. **79**, 014707 (2010).

[30] M. R. Beasley, J. E. Mooij, and T. P. Orlando, Phys. Rev. Lett. **42**, 1165 (1979).

[31] J. M. Kosterlitz and D. J. Thouless, J. Phys. C: Solid State **6**, 1181 (1973).

[32] B. I. Halperin and D. R. Nelson, J. Low Temp. Phys. **36**, 599 (1979).

[33] M. Tinkham, *Introduction to Superconductivity* (Courier Corporation, Chelmsford, MA, 2004).